

## Reactive Sputter-Based Synthesis of HfN Nanofluids

M. Protsak<sup>1</sup>, K. Biliak<sup>1</sup>, D. Nikitin<sup>1</sup>, P. Pleskunov<sup>1</sup>, S. Ali-Ogly<sup>1</sup>, M. Tosca<sup>1</sup>, T. Košutová<sup>1</sup>, M. Cieslar<sup>1</sup>, A. Choukourov<sup>1</sup>

<sup>1</sup> Charles University, Faculty of Mathematics and Physics, Department of Macromolecular Physics, Prague, Czech Republic

**Abstract:** Instead of well-known HfN thin films, this work investigates the preparation of HfN nanoparticles (NPs) using reactive sputtering of Hf in Ar/N<sub>2</sub> mixtures in the configuration of a gas aggregation cluster source. Depending on the Ar/ N<sub>2</sub> ratio, NPs with different nitrogen content can be prepared, including stoichiometric HfN. The NPs can be directly loaded into vacuum-compatible liquids to produce plasmonic nanofluids that can be potentially used in various optoelectronic applications.

**Keywords:** reactive magnetron sputtering, nanoparticles, gas aggregation cluster source.

### 1. Introduction

Group IV transition-metal nitrides (TiN, ZrN, and HfN) have often been considered as refractory proxies for plasmonic metals. In addition to localized surface plasmon resonance (LSPR) in the visible or near-IR range, they benefit from high melting temperature, high chemical stability, and high hardness. Such a combination of properties makes these materials attractive for numerous applications. For example, ZrN and HfN were considered as refractory alternatives to silver for solar mirror applications [1]. In most cases, these materials were prepared in the form of thin films using reactive magnetron sputtering. There are also reports showing that TiN, ZrN, and HfN NPs may be excitingly useful in a number of other LSPR applications such as surface-enhanced Raman scattering for chemical sensing and surface plasmon waveguides [2,3]. Furthermore, nanofluids based on TiN, ZrN, and HfN NPs were suggested for use as direct solar collectors [3]. Few studies have explored the synthesis of transition metal nitride NPs using low-temperature plasma methods [4,5]. Recently, we have shown that reactive magnetron sputtering can be adapted to the synthesis of Ta oxynitride NPs [6]. Following these earlier results, we present the research on reactive magnetron sputtering of Hf. The aim was to produce HfN NPs and load them into vacuum-compatible host liquids with the formation of nanofluids.

### 2. Experimental

Experiments were performed using a gas aggregation cluster source equipped with a 3-inch planar magnetron with a 3-mm thick Hf target (Fig. 1). The magnetron was powered by a power source at dc = 500 mA. The GAS was vertically attached to a deposition chamber through a conical nozzle with an orifice of 2 mm in diameter. Both the GAS and the deposition chamber were pumped by rotary and turbomolecular pumps to a base pressure of 10<sup>-4</sup> Pa. Ar and N<sub>2</sub> were introduced into the GAS via individual flow controllers. The flow rate of Ar was fixed at 24.0 sccm, while the flow rate of N<sub>2</sub> was variable to produce gas mixtures of different nitrogen content. The pressure in the GAS was 81 Pa.

The deposition rate of NPs was measured using QCM installed in the deposition chamber. Si wafers and TEM grids were used as substrates. These were introduced into

the deposition chamber through a loadlock at a distance of 10 cm below the orifice. In a separate series of experiments, Petri dishes with 2 ml of vacuum-compatible liquids were used to deposit NPs directly on the liquid surface. Poly(ethylene glycol) (PEG, 400 g/mol), paraffin, and pentaphenyl trimethyl trisiloxane (PTT) were used as host liquids.

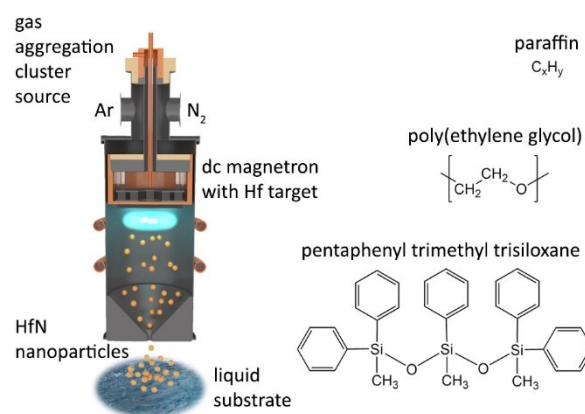


Fig. 1 Scheme of gas aggregation cluster source for sputter-based synthesis of HfN NPs and their loading into host liquids.

### 3. Results and discussion

Sputtering was initiated in Ar without N<sub>2</sub> and a stable deposition of NPs was obtained. Then N<sub>2</sub> was added to Ar in sequential steps, each lasting 1 min. At the end of each step, the deposition rate and magnetron bias were measured (Fig. 2). At low N<sub>2</sub> concentrations, sputtering proceeds in a metal mode, so that the deposition rate and bias remain constant. However, reaching the N<sub>2</sub> concentration beyond 9 vol. % results in an abrupt decrease of the deposition rate, which is accompanied by an increase in bias. Under these conditions, the magnetron enters the reactive mode, with a partially poisoned state and a lower sputtering yield of the target. Under a reversed protocol of a decreasing N<sub>2</sub> concentration, hysteresis in the deposition rate and bias can be observed, evidencing that the process of the NP synthesis obeys the same phenomenology as in the case of well-investigated processes of thin-film deposition.

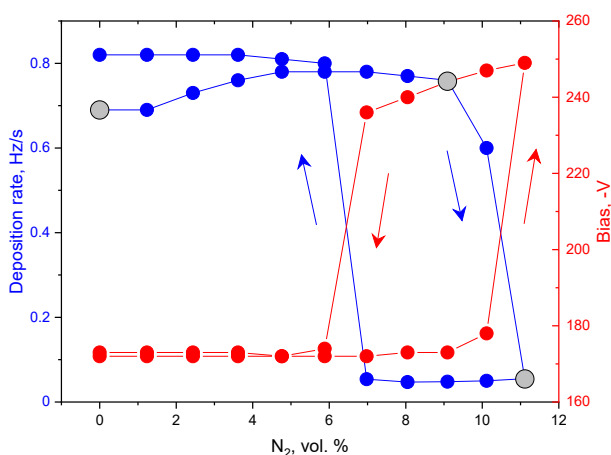


Fig. 2 Dependence of the deposition rate of NPs and magnetron bias on the  $N_2$  concentration in the GAS.

For the following analysis, the samples were prepared in three different Ar/ $N_2$  mixtures shown by gray circles in Fig. 2: Hf NPs deposited in Ar without  $N_2$ , at 9 vol. % of  $N_2$  (just before the target poisoning occurs, sub-HfN) and at 11 vol. % of  $N_2$  (just after the target poisoning occurs, HfN). In all three cases, NPs were successfully synthesized, as is evident from the TEM images shown in Fig. 3. The NPs produced in the metallic mode are characterized by the mean size of 25 nm, while the NPs obtained in the reactive mode have a smaller mean size of 15 nm. A more detailed analysis was performed using STEM-EDS on single particles. After storage in air, the NPs become partially oxidized as is evident from the green shell, the green color corresponding to the signal from O. The core of the NP prepared in Ar is purely metallic, with the blue color corresponding to Hf. For NPs prepared in Ar/ $N_2$  mixtures, the core part is a combination of blue and cyan colors, which indicates the presence of HfN.

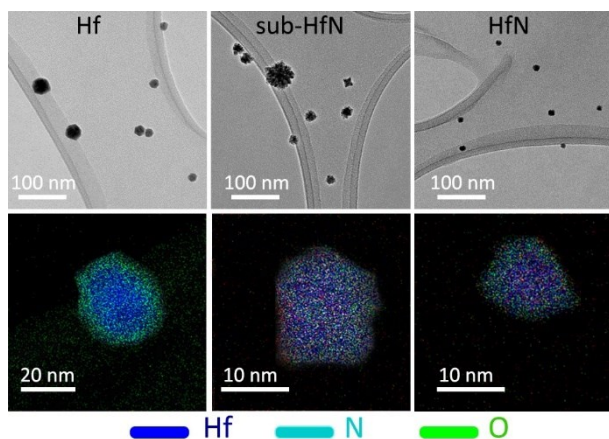


Fig. 3 TEM and STEM-EDS images of Hf NPs prepared in Ar and HfN NPs prepared in Ar/ $N_2$  mixtures before (sub-HfN) and after (HfN) the target poisoning.

Under a given resolution of STEM-EDS, it is impossible to distinguish whether the nitrogen content is different in sub-HfN and HfN NPs. XPS analysis was performed to investigate the chemical transformations in more detail (Fig. 4). The XPS Hf 4f spectra were acquired immediately after sample preparation without breaking the vacuum. These were compared to XPS spectra measured on the same samples but after one day of storage in air.

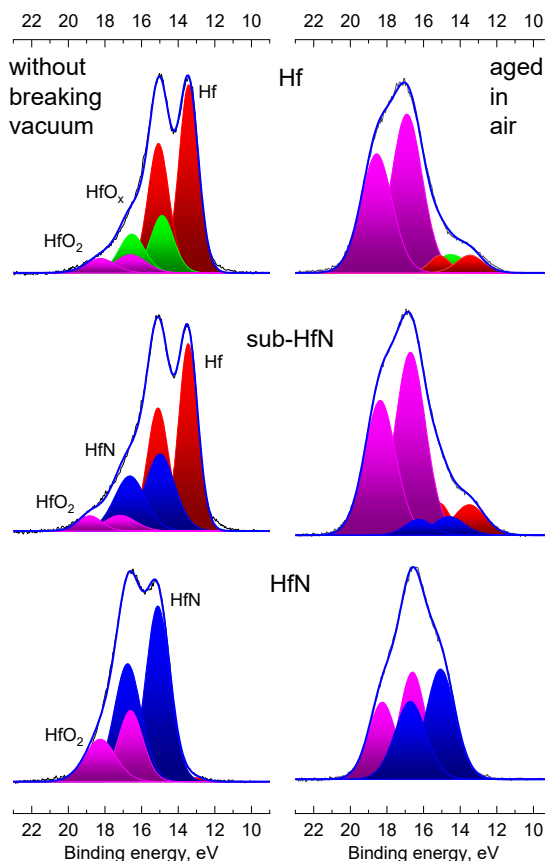


Fig. 4 XPS Hf 4f spectra acquired on Hf, sub-HfN and HfN NPs immediately after sample preparation without breaking vacuum and after one day storage in air.

The spectrum of as-deposited Hf NPs is dominated by a spin-split doublet of metallic components, with a small contribution from Hf suboxides and  $HfO_2$ . Storage in air results in the formation of the oxide shell, which manifests itself through a substantial enhancement of the signal from  $HfO_2$  and attenuation of the signal from metal Hf.

For as-deposited sub-HfN NPs, the signal from N was detected in the survey spectrum, and, hence, the doublet between Hf and  $HfO_2$  was assigned to HfN. Nevertheless, the most dominant signal still comes from metal Hf in this case, and the NPs remain substoichiometric. A similar oxidation of the sub-HfN NPs was observed after aging in air.

For HfN NPs, only two pairs of peaks are detected belonging to dominant HfN and minor  $HfO_2$ , whereas no

signal from the metal Hf can be observed. The surface of these NPs is also prone to oxidation; however, the signal from HfN remains high even after storage in air. The presence of HfN was further confirmed by XRD measurements (not shown) that detected a well-resolved crystallographic pattern perfectly matching that of fcc lattice of stoichiometric HfN.

Using our recently developed methodology [7,8], we prepared nanofluids by loading Hf, sub-HfN, and HfN NPs directly into liquid PEG. Fig. 5a shows the UV-vis optical transmittance spectra of these nanofluids measured against the control sample of blank PEG. The Hf and sub-HfN nanofluids reveal similar spectra with transmittance monotonously decreasing toward the blue range. On the contrary, HfN NPs demonstrate a strong transmittance minimum in the IR/near-IR range, which can be attributed to LSPR. The difference between the nanofluids is also evident to the naked eye in the photos of their vials: Hf and sub-HfN appear brownish, whereas HfN exhibit a bluish color.

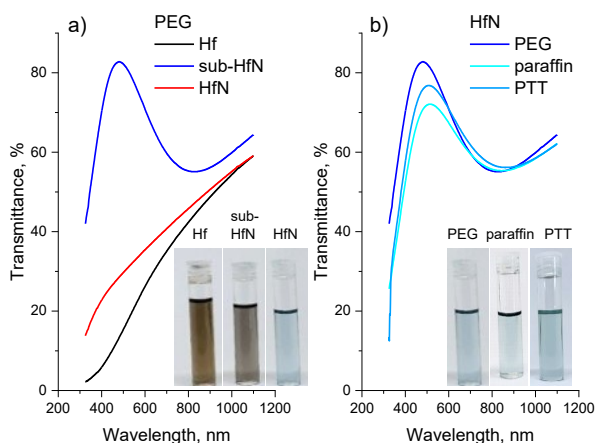


Fig. 5 UV-vis optical transmittance spectra of: a) Hf, sub-HfN and HfN NPs loaded into PEG400; b) HfN NPs loaded into PEG400, paraffin and PTT.

The HfN NPs were also loaded into liquid paraffin and PTT and very similar optical spectra were obtained (Fig. 5b). For all three host liquids studied, the same LSPR band can be observed, which results in the same bluish color of these nanofluids. Thus, the dielectric properties of the host liquids do not seem to play a significant role in the optoelectronic properties of HfN NPs.

#### 4. Conclusions

Magnetron sputtering of Hf under an increased pressure of Ar results in the formation of Hf NPs in the gas phase. Adding N<sub>2</sub> to Ar leads to the incorporation of nitrogen into NPs; however, they remain substoichiometric until the target poisoning occurs. Although under poisoning conditions reactive sputtering is less efficient and proceeds with a lower deposition rate, the resultant NPs consist of nearly stoichiometric ZrN. All types of NPs partially

oxidize with the formation of an oxide/oxy-nitride shell when exposed to air. Nevertheless, HfN NPs demonstrate optical activity, showing LSPR in the infrared/near-IR range. The NPs can be loaded directly from the gas phase into vacuum-compatible liquids to produce nanofluids. This method may be attractive for the production of new liquid materials for future optoelectronic applications.

#### 5. Acknowledgements

The work was supported by the grant GACR 21-12828S from the Czech Science Foundation. K.B. acknowledges the support from the Grant Agency of Charles University through a grant GAUK 298722.

#### 6. References

- [1] P. Das, B. Biswas, K.C. Maurya, M. Garbrecht, B. Saha, Refractory Plasmonic Hafnium Nitride and Zirconium Nitride Thin Films as Alternatives to Silver for Solar Mirror Applications, *ACS Appl. Mater. Interfaces*. 14 (2022) 46708–46715.
- [2] M. Kumar, N. Umezawa, S. Ishii, T. Nagao, Examining the Performance of Refractory Conductive Ceramics as Plasmonic Materials: A Theoretical Approach, *ACS Photonics*. 3 (2016) 43–50.
- [3] C.V.P. Vital, S. Farooq, R.E. de Araujo, D. Rativa, L.A. Gómez-Malagón, Numerical assessment of transition metal nitrides nanofluids for improved performance of direct absorption solar collectors, *Appl. Therm. Eng.* 190 (2021).
- [4] S. Exarhos, A. Alvarez-Barragan, E. Aytan, A.A. Balandin, L. Mangolini, Plasmonic Core-Shell Zirconium Nitride-Silicon Oxynitride Nanoparticles, *ACS Energy Lett.* 3 (2018) 2349–2356.
- [5] M. Dasog, Transition Metal Nitrides Are Heating Up the Field of Plasmonics, *Chem. Mater.* (2022).
- [6] P. Pleskunov, T. Košutová, M. Vaidulych, D. Nikitin, Z. Krtouš, S. Ali-Ogly, K. Kishenina, R. Tafiichuk, H. Biederman, I. Gordeev, J. Drewes, I. Barg, F. Faupel, M. Cieslar, R. Yatskiv, Y. Pihosh, V. Nandal, K. Seki, K. Domen, A. Choukourov, The sputter-based synthesis of tantalum oxynitride nanoparticles with architecture and bandgap controlled by design, *Appl. Surf. Sci.* 559 (2021) 149974.
- [7] A. Choukourov, D. Nikitin, P. Pleskunov, R. Tafiichuk, K. Biliak, M. Protsak, K. Kishenina, J. Hanuš, M. Dopita, M. Cieslar, T. Popelář, L. Ondič, M. Varga, Residual- and linker-free metal/polymer nanofluids prepared by direct deposition of magnetron-sputtered Cu nanoparticles into liquid PEG, *J. Mol. Liq.* 336 (2021).
- [8] K. Biliak, D. Nikitin, S. Ali-Ogly, M. Protsak, P. Pleskunov, M. Tosca, A. Sergievskaya, D. Cornil, J. Cornil, S. Konstantinidis, T. Košutová, Z. Cernochova, P. Štěpánek, J. Hanuš, J. Kousal, L. Hanykova, I. Krakovský, A. Choukourov, Plasmonic Ag/Cu/PEG Nanofluids Prepared when Solids Meet Liquid in the Gas Phase, *Nanoscale Adv.* accepted (2023). doi:10.1039/D2NA00785A.